Journal of ELECTRONIC MATERIALS, Vol. 48, No. 9, 2019
https://doi.org/10.1007/s11664-019-07243-1

Modeling and Fuzzy MPPT Controller Design for Photovoltaic Module Equipped with a Closed-Loop Cooling System

M. BECHOUAT,[1,5] M. SEDRAOUI,[1,6] C.-E. FERAGA,[2,7] M. AIDOUD,[3,8] and S. KAHLA[4,9]

1.—Laboratoires des Télécommunications LT, Department of Electronic and Telecommunication, University 8 Mai 1945 Guelma, Guelma, Algeria. 2.—Laboratory of Electrical Engineering LGEG, University 8 May 1945 of Guelma, Guelma, Algeria. 3.—Laboratory of Automatic and Informatics of Guelma LAIG, University 8 May 1945 of Guelma, Guelma, Algeria. 4.—Research Center in Industrial Technologies, CRTI, Algiers, Algeria. 5.—e-mail: mohcene.oui@gmail.com. 6.—e-mail: msedraoui@gmail.com. 7.—e-mail: chferaga@yahoo.fr. 8.—e-mail: aidoudm@gmail.com. 9.—e-mail: samikahla40@yahoo.com

Electrical energy generated by a photovoltaic (PV) panel depends heavily on two climatic conditions: total solar irradiance and absolute temperature. If high intensity of the solar illumination contributes positively to increasing electrical power, a high degree of absolute temperature has, by contrast, a negative effect on its electrical characteristic. In this paper, the electrical efficiency provided by a conventional PV panel is enhanced using the proposed photovoltaic thermal (PVT) panel. The latter contains serpentines fed by a water tank, which allows cooling its PV cells at high temperature. Accordingly, the desired enhancement needs two main requirements: an efficient PVT panel model that accurately describes the actual PVT panel behavior and an efficient controller that correctly tracks the maximum power point tracking (MPPT). For this reason, a number of experimental test data is firstly recorded from an actual ISOFOTON I-50-PVT module under different climatic conditions. Afterward, the recorded data are fitted by the Curve Fitting Toolbox (CF-Tool), creating therefore a 2-dimensional lookup table, used in the following step. Next, the fuzzy logic control (FLC) strategy is employed to synthesize the proposed MPPT-FLC controller, which should ensure a good extraction of the maximal electrical power. To validate the effectiveness of the proposed MPPT-FLC controller based on a 2-dimensional lookup table, the obtained performance is compared, in terms of electrical power and duty cycle, to those provided by an MPPT-FLC controller for a conventional PV panel in various climatic conditions.

Key words: Photovoltaic thermal system, 2-Dimensional lookup table, fuzzy logic control, maximum power point tracking

INTRODUCTION

Solar energy offers the benefits of being a clean and inexhaustible renewable energy that can be used in many industrial and domestic applications such as, heating systems, electrical networks, street lighting, battery charging and autonomous PV pumping systems.[1,2] It is one of the most promising renewable energies; it is clean, inexhaustible and free to harvest.[1,3] Indeed, the solar cell converts light energy into electricity whose electrical characteristics may vary depending on weather conditions. It is often manufactured using a semiconductor such as silicon, germanium, gallium, arsenide, etc.[3,4]

(Received October 6, 2018; accepted April 19, 2019; published online April 30, 2019)

In the modeling stage of actual PV cell behavior, several PV panel models have been proposed, in which the model parameters are determined using either analytical approaches or experimental test data. Among scholars interested by this area, El-Naggar, K., AlRashidi, M., AlHajri, M., Al-Othman, A., 2012 used the simulated annealing (SA) optimizer to identify the PV cells parameter where a mathematical PV model is represented by an equivalent circuit based on a single-diode model and two-diode model.[5] Ismail, M., Moghavvemi, M., Mahlia, T., 2013 identified these parameters by solving the modeling problem using a global optimization based-genetic algorithm (GA).[6] Askarzadeh, A., dos Santos Coelho, L., 2015 enhanced the accuracy of the PV panel model in different operating conditions using the simplified bird mating optimizer (SBMO).[7]

In the same vein, several MPPT technologies PV-based models have been proposed to operate well the actual PV panel at maximum power point (MPP). Indeed, various MPPT strategies have been reported in the literature, and in which the output power of actual PV panels is ensured despite changes in solar irradiance or temperature.[3,7] Among scholars interested in this field, Safari, A., Mekhilef, S., 2011 presented a simulation and hardware implementation of incremental conductance algorithm (INC), ensuring therefore a good extraction of the MPPT for actual PV panels. The obtained tracking dynamic was guaranteed by applying a proportional integrator (PI) controller on a buck converter, regardless of the direct use of pulse width modulation (PWM).[8] Abdelsalam et al.[9] proposed a high-performance adaptive perturb and observe (P&O) MPPT technique for PV panel based micro-grids. The proposed technique allows ensuring a steady state performance without oscillations around the MPP.[9] Bendib et al.[10] proposed an advanced FLC- based MPPT controller for a stand-alone PV panel. Indeed, the MPPT-FLC controller is synthesized to identify the MPP, providing therefore an adequate operating voltage.[10]

It should be noted that all previous modeling approaches and MPPT controller synthesis techniques have been conducted only for standard PV panels. However, modeling and MPPT controller synthesis for PVT panels represent the main contribution of this paper. For this reason, an adequate PVT panel model based on a 2-Dimensional lookup table is used in modeling the actual PVT panel behavior using Curve Fitting Toolbox, and the MPPT-FLC controller is accordingly synthesized. The proposed MPPT scheme should ensure a good duty cycle, providing, thus, good tracking of the MPP for the PVT panel. The obtained performance is then compared to that provided by standard PV panels controlled by an MPPT-FLC controller. The results highlight improved performance in terms of maximum power output, duty cycle and efficiency.

DESIGN OF THE PVT PANEL MODEL

PVT Panel Model Based Single-Diode Electrical Circuit

In general, the PVT cell is made of a semiconductor material which absorbs light energy and converts it into electrical current. The solar cells are generally connected in series and in parallel, and then encapsulated in glass for a PVT panel. It consists of modules interconnected to form a power generation unit. This can ensure high compatibility with conventional electrical equipment. Moreover, these modules can also be connected in series-parallel to increase the output power. Furthermore, the interconnected modules are mounted on metal supports and inclined at a desired angle depending on the location; this set is often called module field.[8,9,11]

Usually, the actual behavior of PVT cells can be modeled in the same way as that of PV cells. This can be done using the following single-diode equivalent circuit model.[12,13]

According to Fig. 1, The output current I_{PVT_c} generated by the PVT cell model is expressed using the Eq. 1[14–16]:

$$I_{PVT_c} = I_{ph} - I_{D_v} - I_{sh}, \tag{1}$$

where I_{PVT_c}, I_{D_v} and I_{sh} denote, respectively, the current generated by the incident light, the current flowing through the diode D_v and the current flowing through the shunt resistance R_p. Using the Shockley equation for the diode current and substituting the shunt resistance current, Eq. 1 is rewritten as Eq. 2[14,16]:

$$I_{PVT_c} = I_{ph} - I_0\left(-1 + e^{\frac{V_{PVT_c}+R_s \cdot I_{PVT_c}}{n \cdot V_t}}\right) - \frac{V_{PVT_c} + R_s \cdot I_{PVT_c}}{R_p}, \tag{2}$$

where n denotes the diode quality factor of the P–N junction, V_{PVT_c} is the output voltage provided by the PVT cell model. The thermal voltage V_t subjected to any temperature T, is defined by the following equation:

$$V_t = \frac{k \cdot T}{q}, \tag{3}$$

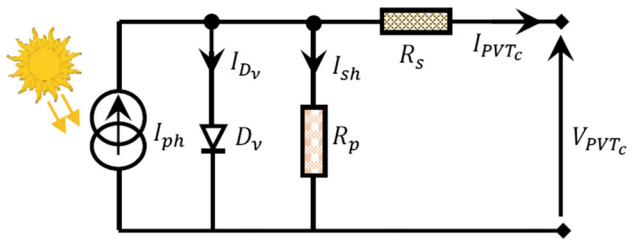

Fig. 1. Equivalent electrical circuit based-single diode for PV/PVT cell.

where q and k denote, respectively, the electron charge and Boltzmann constant. In addition, the reverse saturation current I_0 of the diodes D can be found using the information from the datasheet given by:

$$I_0 = I_{0,n} = \left(\frac{T}{T_n}\right)^{\frac{3}{n}} e^{\frac{q \cdot V_g}{n \cdot k}\left(\frac{1}{T_n} - \frac{1}{T}\right)}, \tag{4}$$

where V_g denotes the band-gap energy in the solar cell. $I_{0,n}$ is the diode saturation current given at STC. It can be found using the following equation:

$$I_{0,n} = \frac{I_{sc,n}}{-1 + e^{\frac{V_{oc} + K_{V_{oc}}(T - T_n)}{n \cdot V_t}}}. \tag{5}$$

Here, V_{oc} denotes the solar cell open-circuit voltage, $I_{sc,n}$ is the solar cell short-circuit current and $K_{V_{oc}}$ is the open-circuit voltage temperature coefficient. All previous parameters are given at STC, i.e., $T_n = 25°\text{C}$ and $G_n = 1000\,\text{W/m}^2$. It should be noted that the photocurrent I_{ph}, given in Eq. 1, depends on irradiance intensity and cell temperature. It is computed by the following equation:

$$I_{ph} = \frac{G}{G_n}\left(I_{sc,n} + K_{I_{sc}}(T - T_n)\right), \tag{6}$$

where $K_{I_{sc}}$ denotes the short-circuit current temperature coefficient of the solar cell. In general, the PVT panel model is built by connecting several PVT cells in series and parallel. Furthermore, the output current and output voltage generated by the PVT panel model, arranged in N_p parallel and N_s series cells, can be expressed using the Eqs. 7 and 8[16]:

$$I_{PVT} = N_p \cdot I_{PVT_c}, \tag{7}$$

$$V_{PVT} = N_s \cdot V_{PVT_c}, \tag{8}$$

where the final mathematical equation connecting I_{PVT_c} by V_{PVT_c} is found by substituting Eqs. 7 and 8 in Eq. 2. It yields also Eq. 10[16]:

$$I_{PVT} = N_p \cdot I_{ph} - N_p \cdot I_0\left(-1 + e^{\frac{\frac{V_{PVT}}{N_s} + \frac{R_s}{N_p} I_{PVT}}{n \cdot V_t}}\right) - \frac{\frac{N_p}{N_s} \cdot V_{PVT} + R_s \cdot I_{PVT}}{R_p}. \tag{9}$$

PVT Panel Model-Based Experimental Test Data

Curve Fitting Tool is a powerful algorithm that allows creating a suitable PVT panel model using experimental test data. This tool allows modeling the recorded experimental test data by a Simulink 2-Dimensional lookup table. This can be done when the following steps are achieved:

Step1: Open Curve Fitting Tool and load the recorded data to be fitted;
Step2: Put the measured solar irradiance vectors in *xdata* box, the measured output voltage vectors in *ydata* box and the measured output current vectors in *zdata* box;
Step3: Creates a fit-object by selecting one of four fit-types: *Custom Equation*; *Interpolant*; *Lowess* and *Polynomial*;
Step4: Save the fitted array data and use them to parameterize a Simulink 2-Dimensional lookup Table block.

SYNTHESIS OF THE MPPT CONTROLLER

The interface between the PVT panel model and the system load is commonly performed using various power electronic circuits.

Figure 2 shows the standard MPPT configuration excited by total solar irradiance and absolute temperature signals.

According to Fig. 2, the standard MPPT configuration consists of a PVT panel modeled by a Simulink 2-Dimensional lookup table. It is associated with a DC-DC step-up converter connected to a system load. This converter is commonly used to boost the PVT panel DC voltage and perform as well the MPPT task of extracting maximum power where some climatic conditions are considered. It should be noted that a good performance provided by MPPT configuration depends heavily on duty cycle quality that should ensure a good extraction of the maximum power from the PVT panel. In this paper, this above mentioned objective is ensured by synthesizing an efficient MPPT controller using fuzzy logic control strategy.[14,15]

Synthesis of the MPPT Fuzzy Logic Controller

In this section, the controller synthesis step is performed by fuzzy logic based control. Indeed, the synthesized controller has the ability to reduce the oscillations of the output power when the MPP is reached. This increases the power loss in the PVT panel, thus reducing its efficiency. The main idea proposed in synthesizing a MPPT-FLC controller lies in determining the optimal duty cycle (D) from two inputs: error input (E) and change in error input (ΔE) at sample time (k). These are expressed by Eqs. 10 and 11[16,17]:

$$E(k) = \frac{P_{pv}(k) - P_{pv}(k-1)}{V_{pv}(k) - V_{pv}(k-1)}, \tag{10}$$

$$\Delta E(k) = E(k) - E(k-1), \tag{11}$$

where $P_{pv}(k)$ denotes the instant power generated by the PVT panel. The MPPT-FLC controller determines, at each sample time (k), the next action required from the fuzzy knowledge base and adjusts

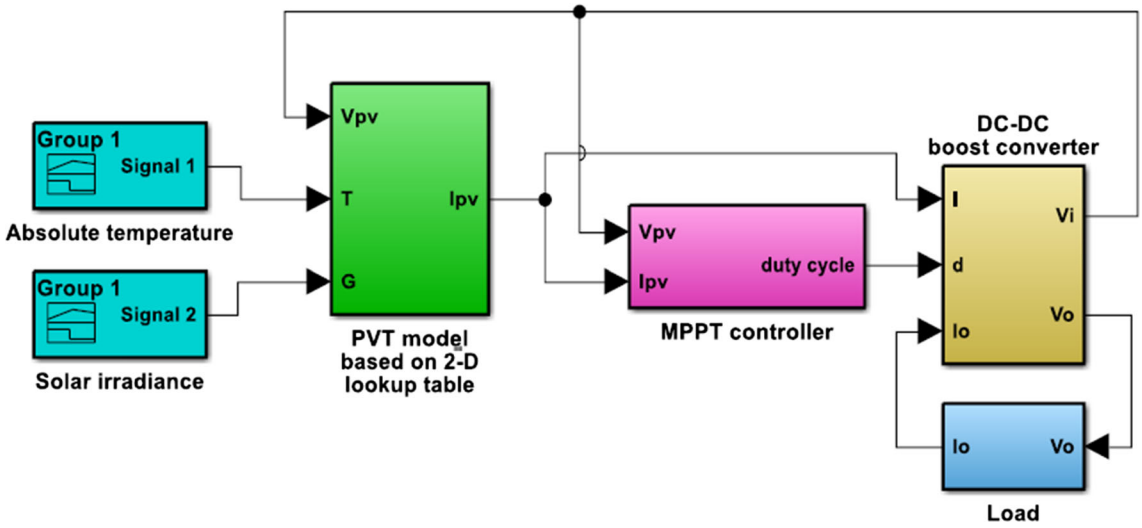

Fig. 2. Standard MPPT configuration.

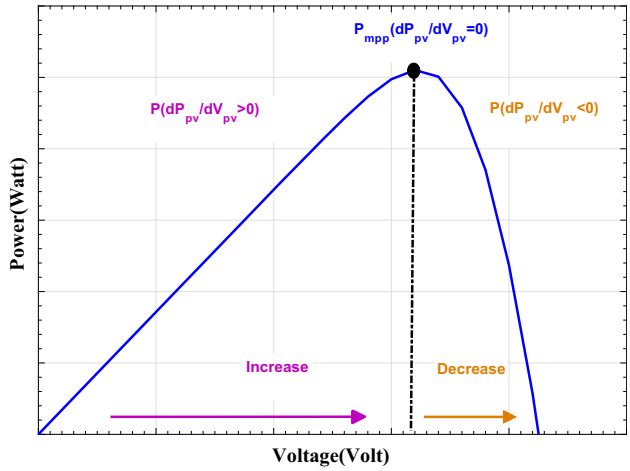

Fig. 3. Power-voltage characteristic of a PVT panel.

duty cycle of the PWM generator to set the operating point of the system to MPP. In the other words, when the term (dP_{pv}/dV_{pv}) is greater than zero, the MPPT-FLC controller changes the duty cycle (D) to increase (V_{pv}) until (P_{pv}) reaches (P_{mpp}) or (dP_{pv}/dV_{pv}) equals zero. Otherwise, when the term (dP_{pv}/dV_{pv}) is less than zero, the MPPT-FLC controller changes (D) to decrease (V_{pv}) until (P_{pv}) reaches (P_{mpp}). This process can be illustrated by Fig. 3.[18,19]

In general the synthesis of the MPPT-FLC based fuzzy control is achieved using the following three basic parts: (1) fuzzification, (2) inference engine, and (3) defuzzification.[20,21]

– In the fuzzyfication part, the membership function values are assigned to the linguistic variables, using the five following fuzzy subsets[22]:

NG: *NegativeGreat*;
NP: *NegativeProximate*;
EZ:*EquivalentZero*;
PP: *PositiveProximate*;
PG: *PositiveGreat*.

Table I. Fuzzy rules

ΔEE	*NG*	*NP*	*EZ*	*PP*	*PG*
NG	*NG*	*NG*	*NG*	*NG*	*NG*
NP	*NP*	*NP*	*NP*	*NP*	*NP*
EZ	*EZ*	*EZ*	*EZ*	*EZ*	*EZ*
PP	*PP*	*PP*	*PP*	*PP*	*PP*
PG	*PG*	*PG*	*PG*	*PG*	*PG*

– In the inference engine part, the fuzzy output presents the change in duty cycle (ΔD), computed using the Eq. 12 fuzzy-rule $(\mathbf{R_i})$ type based Mamdani method[20,21]:

$$(\mathbf{R_i}) : if\{E(K)\, is\, x_1\, and\, \Delta E(K)\, is\, x_2\} then\{\Delta D\, is\, x_3\}\,, \tag{12}$$

where $\{x_1, x_2\}$, and x_3 are linguistic terms associated with the input and output variables $\{E, \Delta E\}$ and ΔD respectively. In the inference engine based on the Mamdani method, one of the following fuzzy combination techniques can be used: *Max–Min*, *Max-Prod* and *Somme-Prod*. Here, the fuzzy combination *Min–Max* is used. Furthermore, Table I summarizes the 25 control fuzzy rules, employed for controlling the DC-DC boost converter such as the MPP of the PVT generator when it is reached.[22]

– The deffuzzification part is performed by either the Center of Area (COA) or the Max Criterion

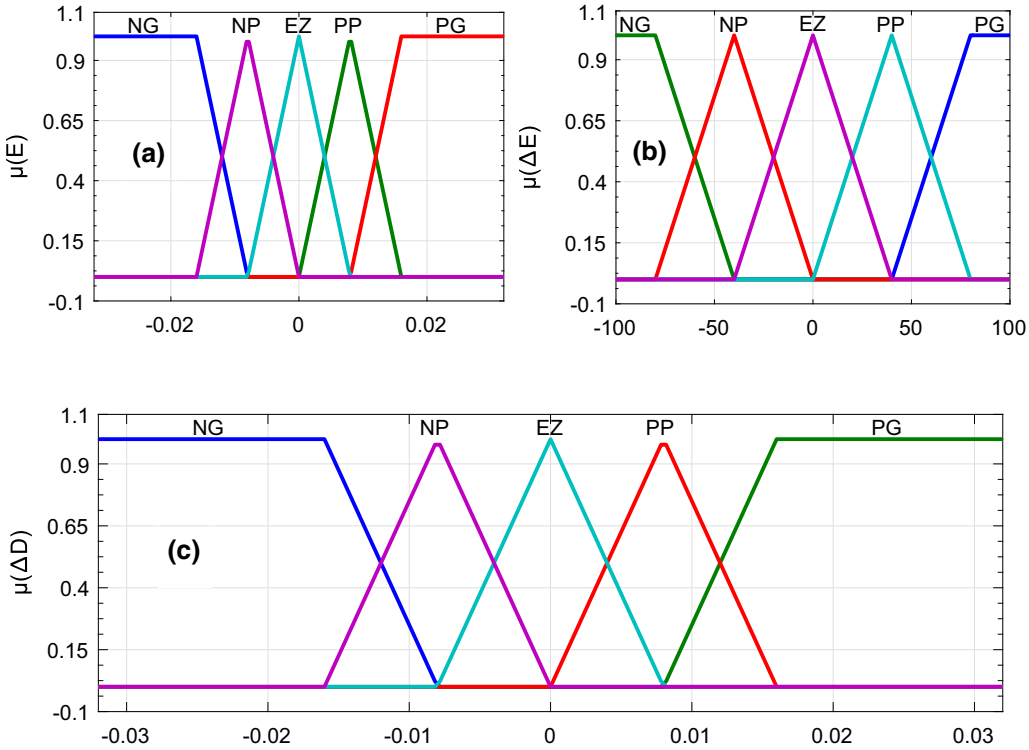

Fig. 4. (a) Membership functions for input variable E. (b) Membership functions for input variable ΔE. (c) Membership functions for output variable ΔD.

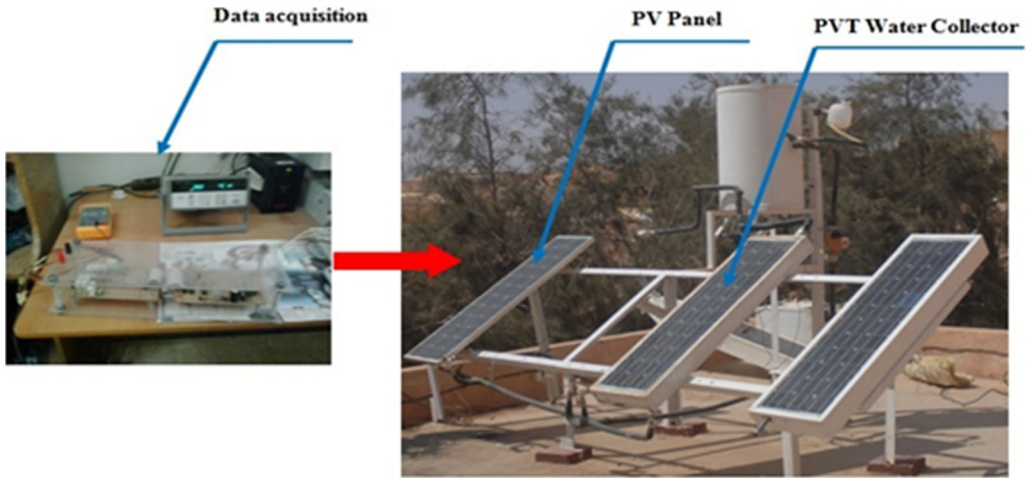

Fig. 5. Experimental prototype of PV and PVT panels.

Method (MCM). Here, the COA deffuzzification method is used to determine (ΔD). It is expressed by Eq. 13[20,21]:

$$\Delta D = \frac{\sum_{j=1}^{n}(\mu(\Delta D_j)\cdot \Delta D_j)}{\sum_{j=1}^{n}\mu(\Delta D_j)}, \qquad (13)$$

where $\mu(X)$ denotes the degree of the membership function of the variable (X). Moreover, Fig. 4 shows the partition of fuzzy subsets and the shape of membership function plots for error E, change in error ΔE and change in duty cycle ΔD respectively.[22]

Finally, the actual duty cycle is computed, at each sample (k) using the Eq. 14:

$$\Delta D(k) = D(k-1) + \Delta D(k). \quad (14)$$

EXPERIMENTAL AND SIMULATION RESULTS

Experimental results

In this part, two solar systems based on the *ISOFOTON I-50* PV modules are modeled and then controlled by the MPPT-FLC controllers. The first solar system is a standard PV panel system whose cells are operated without a cooling system. On the other hand, the proposed PVT panel system is reinforced against high temperatures by means of a closed water circuit.[15]

The abovementioned solar systems are positioned on the building roof of the Center for the Development of Renewable Energies (CDER), Ghardia, Algeria. Furthermore, they are inclined by an angle equal to the latitude of the area and each one has two instruments. The first one is the K-type thermocouple based Campbell *CS215* instrument used to measure the temperature of PV and PVT panels whereas the second one is a solar power meter based Kipp & Zonen *CMP21* pyranometer instrument used to measure total solar irradiance.

The Agilent *34970A* Data Acquisition Control is employed along with a current measurement shunt resistor to record the measured values of current and voltage of the PV and PVT panels with high accuracy. The experimental systems are shown in Fig. 5.[15]

The dimensions of the PV and PVT panels are $1224\,mm \times 1047mm$. The datasheet values of these solar systems are shown in Table II.[19]

The experiment is carried out for nine arbitrarily chosen days during 2017. This allows sweeping the possible variations of the meteorological conditions observed over the year. The measured voltage and measured current were recorded in different weather conditions, as summarized in Table III.

Figures 6 and 7 show the measured I–V characteristics recorded through actual PV and PVT panels under different weather conditions summarized before.

Table II. Datasheet values of *ISOFOTONI-50* PV module

Parameters	Datasheet values
Maximum power P_{max}	39.10 W
Short circuit current	2.99 A
Open circuit voltage	20.80 V
Maximum voltage V_{max}	14.90 V
Maximum current I_{max}	2.620 A
Number of cells	36

DESIGN OF PV AND PVT PANEL MODEL

In the CF-Tool function, a Custom Equation is chosen to fit the experimental test data recorded through the actual PVT and PVT panels where the proposed PVT panel model is designed with the five parameters: a_1, b_1, c_1, d_1, and m_1 whereas the proposed PV panel model is designed with other five parameters a_0, b_0, c_0, d_0, and m_0. Moreover, the proposed mathematical equation for the PVT panel model is expressed as Eq. 15[23–25]:

$$I_{PVT} = f(V_{PVT}, G) = a_1 \cdot G - b_1(-1 + e^{-1+m_1 \cdot V_{PVT}}) - \frac{V_{PVT} + c_1}{d_1}. \quad (15)$$

And the fitting process provides the following solution:

$$(a_1, b_1, c_1, d_1, m_1) = (0.002947, 15.19, -15.77, 3.083, -0.08653), \quad (16)$$

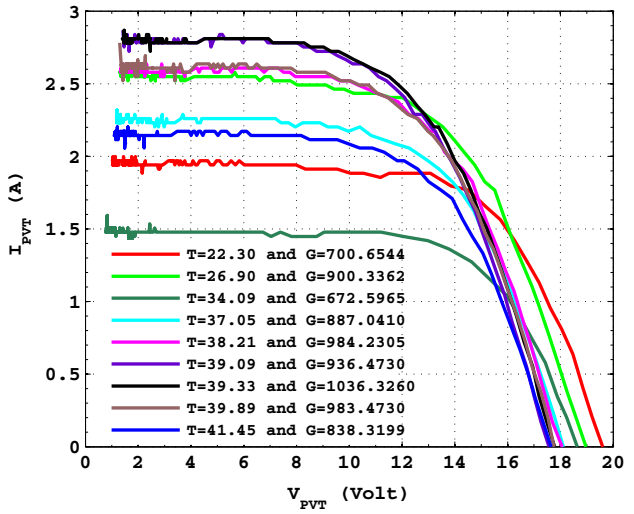

Fig. 6. Measured I–V curves recorded PVT panel.

Table III. Absolute temperature and total solar irradiance recorded over the year 2017

Day	1	2	3	4	5	6	7	8	9
G	700.65	900.33	672.59	878.04	984.23	936.47	1036.32	983.27	838.31
T	22.30	26.90	34.09	37.05	38.21	39.09	39.33	39.89	41.45

where the PVT model accuracy is given by the Root Mean Square Error $RMSE_1 = 0.196$. Figure 8 shows the 3D view of the corresponding 2-Dimensional lookup table data.

Similarly, the CF-Tool function is used to fit the experimental test data recorded through the actual PV system. The PV panel model is created using the same previous fit-type, providing, thus, the Eq. 17[23–25]:

$$I_{PV} = f(V_{PV}, G) = a_0 \cdot G - b_0(-1 + e^{-1+m_0 \cdot V_{PV}}) - \frac{V_{PV} + c_0}{d_0}, \quad (17)$$

where

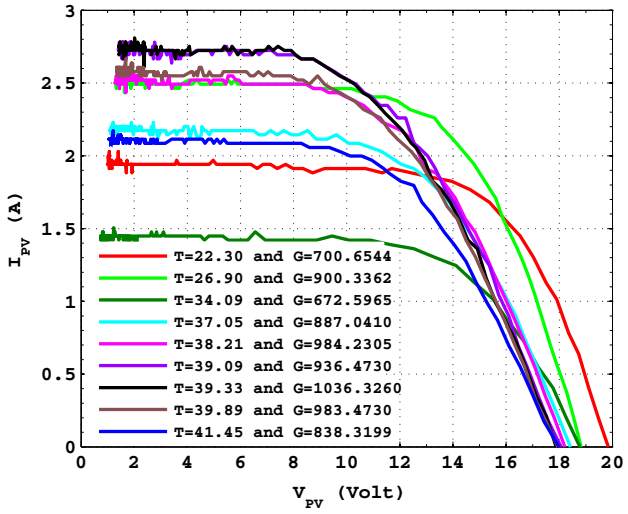

Fig. 7. Measured I–V curves recorded PV panel.

$$(a_0, b_0, c_0, d_0, m_0) = (0.002869, 2.477, -7034, 8551, 0.0532). \quad (18)$$

And the model accuracy is given by $RMSE_0 = 0.2397$.

Synthesis of MPPT-FLC Controller for PV and PVT Panels

Performance assessments in terms of power output and duty cycle for both PV and PVT panels are performed using the MPPT configuration shown in Fig. 9. Accordingly, the Boost parameters are given by[22]:

$L = 350 \times 10^{-6} H, C_1 = C_2 = 560 \times 10^{-6} F, R = 20\,\Omega$.

Furthermore, the MPPT-FLC synthesis controller ensuring a good extraction of the MPP for both previous panels has been previously mentioned. To highlight the good performance of the proposed PVT system, the following simulation is performed for various total solar irradiance values ($600\,W/m^2, 1000\,W/m^2$ and $800\,W/m^2$) at fixed absolute temperature of 25°C (see Fig. 10).

Furthermore, Fig. 10 shows the duty cycles by the MPPT-FLC controller for PV and PVT panels.

According to Figs. 10, 11 and 12, one can clearly see that both PV and PVT panels based on MPPT-FLC controllers can track the maximum power operating voltage point. It can also be observed that the dynamic response and the duty cycle provided by the proposed MPPT-FLC controller are better than those provided by the standard PV panel. This is ensured regardless of the rapid change in total solar radiation. Furthermore, both MPPT-FLC controllers allow reducing the power losses for PV and PVT panels. This can be explained by the complete

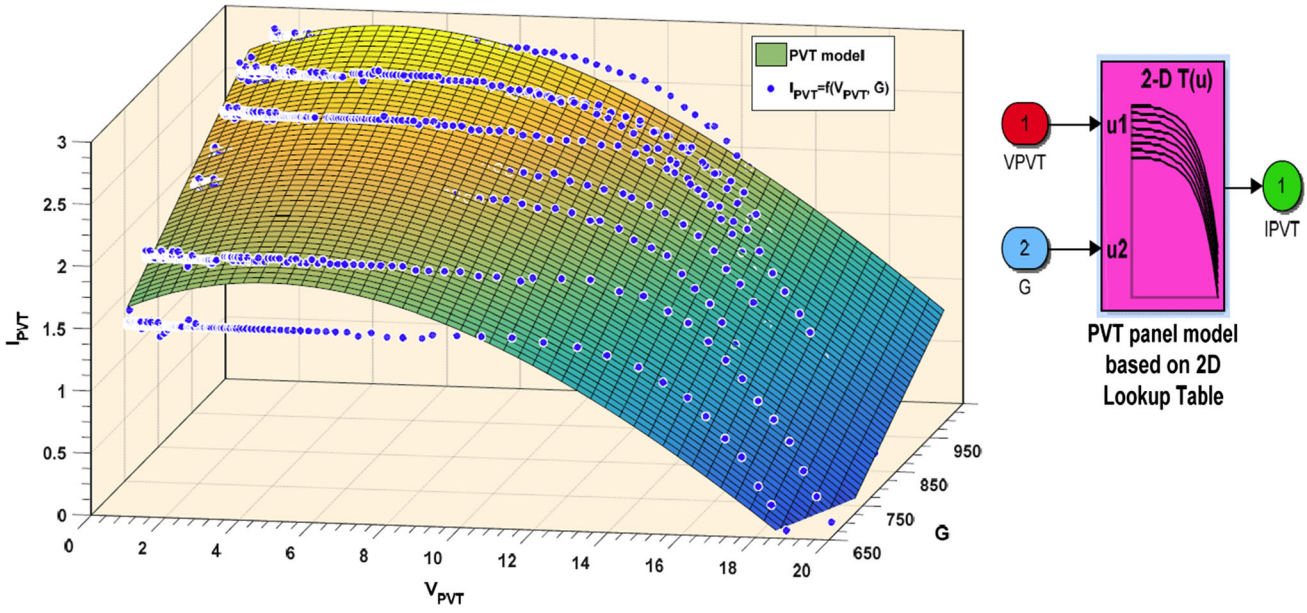

Fig. 8. 3D view of the 2-dimensional lookup table data for the PVT system.

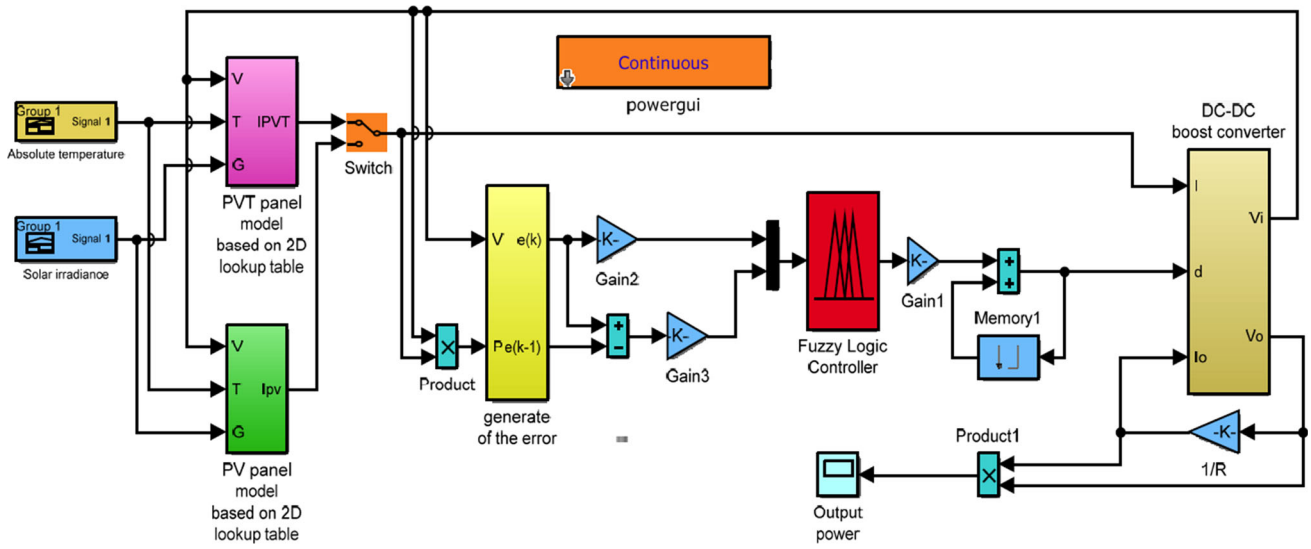

Fig. 9. MPPT-FLC configuration for PV and PVT panels.

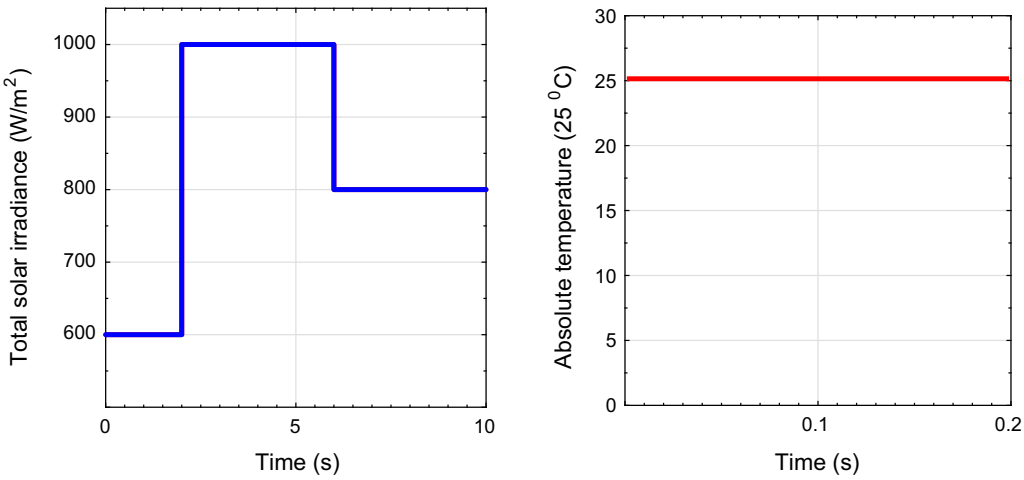

Fig. 10. Constant temperature and variable solar irradiance inputs used to compare the PV and PVT panels.

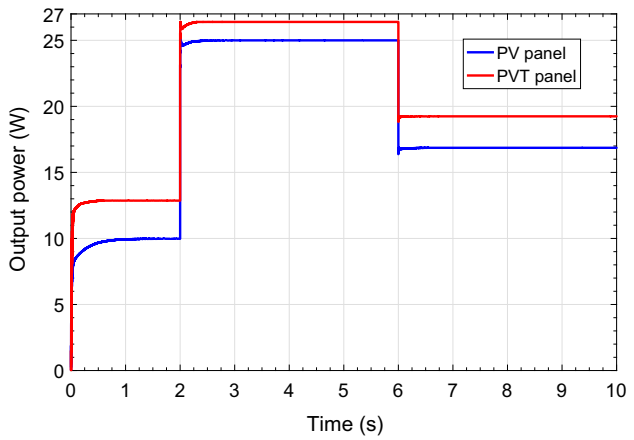

Fig. 11. The corresponding output powers provided by the PV and PVT panels.

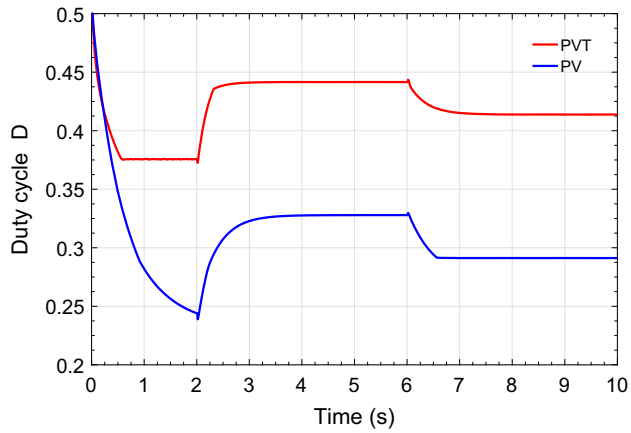

Fig. 12. Duty cycles provided for the PV and PVT panels.

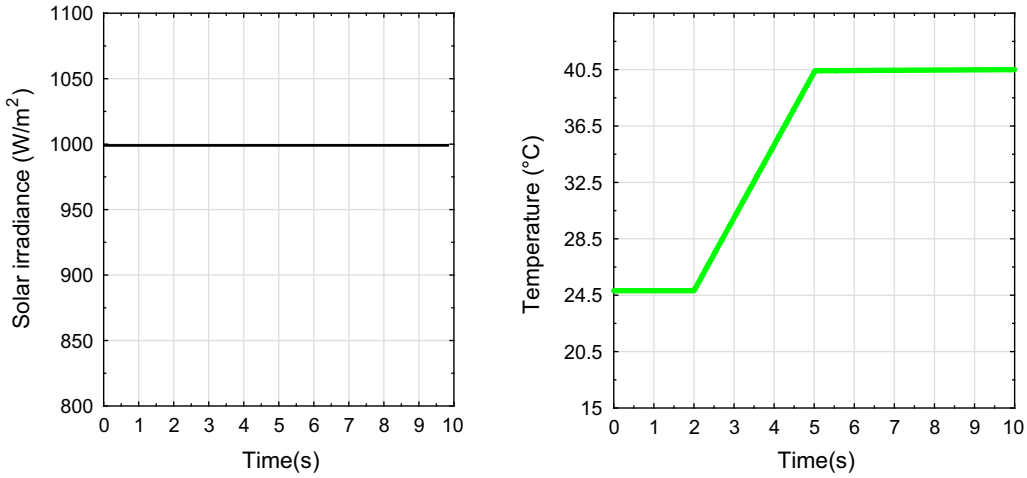

Fig. 13. Variable absolute temperature and constant solar irradiance inputs used to compare the PV and PVT panels.

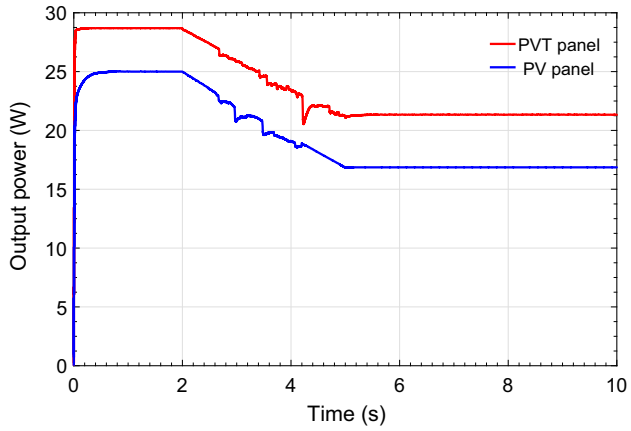

Fig. 14. The corresponding output powers provided by the PV and PVT panels.

absence of oscillation. Now, a rapid increase in cell temperature from 24.5°C to 40.5°C within a time period of 3 s is used whereas the total solar irradiance is kept at a constant value of $1000\,W/m^2$ (see Fig. 13).

Accordingly, the output power provided by the PV and PVT panels is given by Fig. 14

According to Figs. 13 and 14, the output power provided by both PV and PVT panels decreases linearly whereas the proposed PVT panel offers better performance in terms of minimum sensitivity at high absolute temperature and generated power.

CONCLUSION

In this paper, the modeling and synthesis of the MPPT controller for both PV and PVT panels were discussed and analyzed in different weather conditions. In the modeling stage, the curve fitting tool is applied to develop both adequate PV and PVT panel models, in which 2-dimensional lookup table Simulink blocks are derived using experimental test data. These models are then used to synthesize two MPPT-FLC controllers and their performance is evaluated in terms of output power and duty cycle for various climatic variations. As a result, the MPPT-FLC controller synthesized via the PVT panel provided better steady state performance characterized by increased output power, improved duty cycle and rapid achievement of the MPP.

ACKNOWLEDGMENTS

The authors would like to thank the Pervasive Artificial Intelligence PAI group of the informatics department of Fribourg–Switzerland—for their valuable suggestions and comments which helped us to improve this paper. Special thanks to Prof. Béat Hirsbrunner and Prof. Michèle Courant.

AUTHORS' CONTRIBUTION

Mohcene Bechouat, Moussa Sedraoui, Chams-Eddine Feraga, Mohammed Aidoud and Sami Kahla contributed equally in the preparation of this manuscript.

CONFLICT OF INTEREST

The authors declare that there is no conflict of interest.

REFERENCES

1. A. Dolara, S. Leva, and G. Manzolini, *Solar Energy* 119, 83 (2015).
2. L. Fialho, R. Melício, V.M.F. Mendes, A. Estanqueiro, and M. Collares-Pereira, *Sustain. Energy Technol. Assess.* 10, 29 (2015).
3. J.H. Chen, H.T. Yau, and T.H. Hung, *Mechatronics* 25, 55 (2015).
4. A.M. Eltamaly and M.A. Mohamed, *J. Braz. Soc. Mech. Sci. Eng.* 38(4), 1299 (2016).
5. K. El-Naggar, M. AlRashidi, M. AlHajri, and A. Al-Othman, *Solar Energy* 86(1), 266 (2012).

6. M. Ismail, M. Moghavvemi, and T. Mahlia, *Energy Convers. Manag.* 73, 10 (2013).
7. A. Askarzadeh and L. dos Santos Coelho, *Energy Convers. Manag.* 89, 608 (2015).
8. A. Safari and S. Mekhilef, in *Electrical and computer engineering (CCECE), 2011 24th Canadian Conference on* (IEEE, 2011), pp. 000345–000347.
9. A.K. Abdelsalam, A.M. Massoud, S. Ahmed, and P.N. Enjeti, *IEEE Trans. Power Electron.* 26(4), 1010 (2011).
10. B. Bendib, F. Krim, H. Belmili, M. Almi, and S. Boulouma, *Energy Procedia* 50, 383 (2014).
11. Q. Mei, M. Shan, L. Liu, and J. Guerrero, *IEEE Trans. Ind. Electron.* 58, 2427 (2011).
12. A.I. Dounis, P. Kofinas, C. Alafodimos, and D. Tseles, *Renew. Energy* 60, 202 (2013).
13. S. Daraban, D. Petreus, and C. Morel, *Energy* 74, 374 (2014).
14. S. Li, *Solar Energy* 108, 117 (2014).
15. M. Bechouat, A. Younsi, M. Sedraoui, Y. Soufi, L. Yousfi, I. Tabet, and K. Touafek, *Int. J. Energy Environ. Eng.* 8(4), 331 (2017).
16. K.K. Chang, *Solar Energy* 115, 419 (2015).
17. M.A. Eltawil and Z. Zhao, *Renew. Sustain. Energy Rev.* 25, 793 (2013).
18. F. Chekired, C. Larbes, D. Rekioua, and F. Haddad, *Energy Procedia* 6, 541 (2011).
19. A. Messai, A. Mellit, A.M. Pavan, A. Guessoum, and H. Mekki, *Energy Convers. Manag.* 52(7), 2695 (2011).
20. E. Mamdani and S. Assilian, *Int. J. Hum–Comput. Stud.* 51(2), 135 (1999).
21. E. Mamdani and S. Assilian, in *Readings in Fuzzy Sets for Intelligent Systems* (Elsevier, 1993), pp. 283–289.
22. Y. Soufi, M. Bechouat, and S. Kahla, *Int. J. Hydrog. Energy* 42(13), 8680 (2017).
23. M.C. Argyrou, P. Christodoulides, and S.A. Kalogirou, in *2018 IEEE International Energy Conference (ENERGYCON)* (IEEE, 2018).
24. M.R. Islam, A. Mahfuz-Ur-Rahman, M.M. Islam, Y.G. Guo, and J.G. Zhu, *IEEE Trans. Ind. Electron.* 64(11), 8887 (2017).
25. M. Kermadi and E.M. Berkouk, *Renew. Sustain. Energy Rev.* 69, 369 (2017).